ACS OMEGA

Open Access

http://pubs.acs.org/journal/acsodf

Article

DFT Studies of the Photocatalytic Properties of MoS_2-Doped Boron Nitride Nanotubes for Hydrogen Production

Yahaya Saadu Itas, Abdussalam Balarabe Suleiman, Chifu E. Ndikilar, Abdullahi Lawal, Razif Razali, Md Habib Ullah, Hamid Osman, and Mayeen Uddin Khandaker*

Cite This: *ACS Omega* 2023, 8, 38632−38640

Read Online

ACCESS | Metrics & More | Article Recommendations

ABSTRACT: This study investigated the photocatalytic properties of MoS_2-doped boron nitride nanotubes (BNNTs) for overall water splitting using popular density functional theory (DFT). Calculations of the structural, mechanical, electronic, and optical properties of the investigated systems were performed using both the generalized gradient approximation and the GW quasi-particle correction methods. In our calculations, it was observed that only (10, 10) and (12, 12) single-walled BNNTs (SWBNNTs) turned out to be stable toward MoS_2 doping. Electronic property calculations revealed metallic behavior of (10, 10)-MoS_2-doped SWBNNTs, while the band gap of (12, 12) SWBNNT was narrowed to 2.5 eV after MoS_2 doping, which is within the obtained band gaps for other photocatalysts. Hence, MoS_2 influences the conduction band of pure BNNT and improves its photocatalytic properties. The water-splitting photocatalytic behavior is found in (12, 12) MoS_2-doped SWBNNT, which showed higher water oxidation (OH^-/O_2) and reduction (H^+/H_2) potentials. In addition, optical spectral calculations showed that MoS_2-doped SWBNNT had an optical absorption edge of 2.6 eV and a higher absorption in the visible region. All of the studied properties confirmed MoS_2-doped SWBNNT as a better candidate for next-generation photocatalysts for hydrogen evolution through the overall water-splitting process.

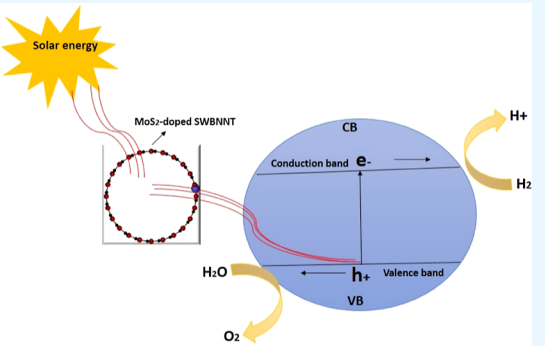

1. INTRODUCTION

Hydrogen storage is a form of chemical energy storage that can be used as a fuel in an internal combustion engine or fuel cell. It is the most abundant element in the universe, accounting for up to 142 MJ kg^{-1}.[1] Due to the overconsumption of fossil fuels and their greater contribution to ecosystem pollution, there is an ongoing fear in the global community.[2] There are many searches and initiatives for alternatives to fossil fuels and conversion to environmental pollution. For example, a study was carried out to reduce atmospheric CO_2 using a Cu−Zn alloy/Cu−Zn aluminate oxide composite electrocatalytic system.[1] Results revealed significant adsorption and activation of CO_2 and the dissociation of H_2O and strengthened the adsorption of CO intermediates. One of the most successful efforts is the discovery of hydrogen fuel, which has greater potential to replace fossil fuels in the near future.[3] This was due to its relatively environmentally friendly properties, which produce water after combustion. In 1972, Fujishima and Honda discovered the production of hydrogen from photocatalytic water splitting by solar radiation.[4] Until now, this method has received much attention as one of the most appropriate processes to solve global energy crises and environmental pollution. Recently, a study was carried out on the evolution of hydrogen under alkaline conditions in Ni−Mo-based electrocatalysts.[2] The results indicated that oxide or hydroxide promotes water dissociation and the alloy accelerates the hydrogen combination.

In order for a semiconductor to act well as a photocatalyst for hydrogen production, (i) the band gap should be larger than the difference between the water oxidation (OH^-/O_2) and reduction potentials (H^+/H_2)[3] and (ii) the water oxidation and reduction potentials should be in the energy gap region between the valence band maxima (VBM) and the conduction band minima (CBM) of the photocatalyst. Several semiconductors with these conditions have been presented in the literature, e.g., TiO_2[4] and Bi_2WO_6.[5]

Although the literature revealed that some theoretical studies on the electronic structure of BNNT[6] materials and the effects of doping on its electronic band structure have been performed, the proofs of the theoretical studies on the electronic and optical structures of the MoS_2-doped and

Received: August 10, 2023
Accepted: September 18, 2023
Published: October 4, 2023

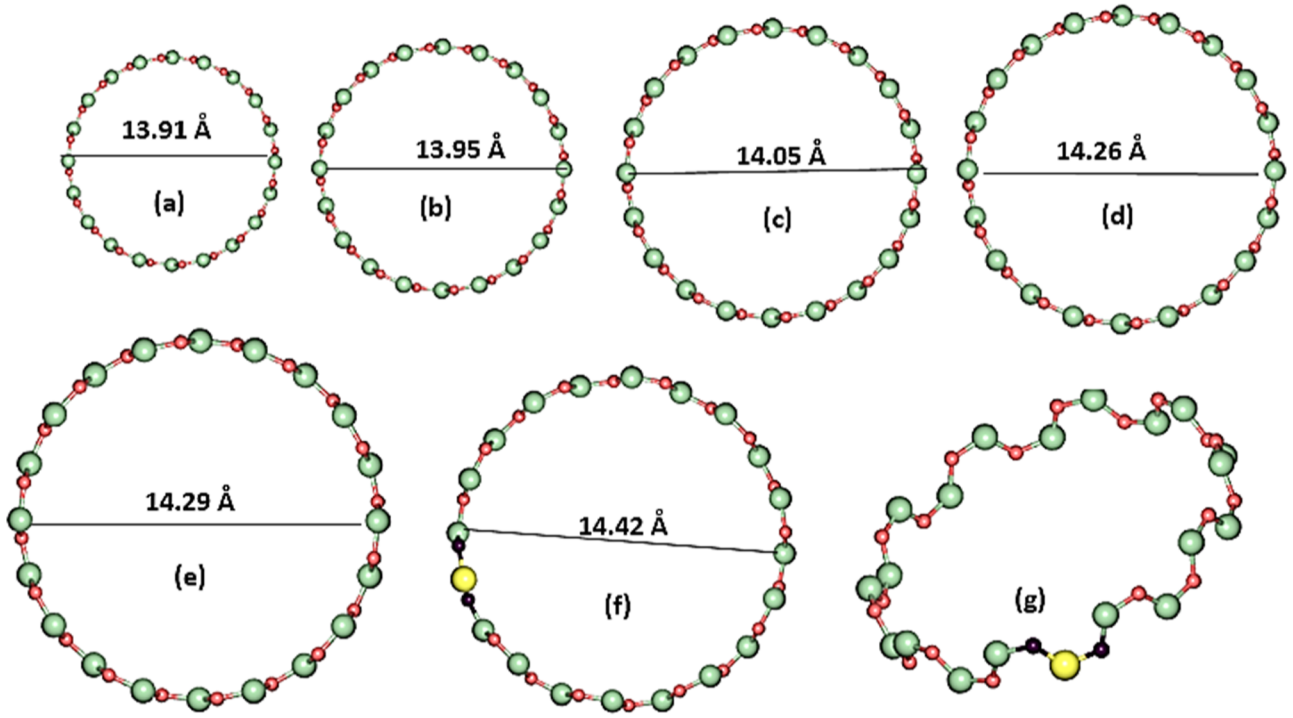

Figure 1. Optimized unit cells of (a) (8, 8) SWBNNT, (b) (9, 9) SWBNNT, (c) (10, 10) SWBNNT, (d) (11, 11) SWBNNT, (e) (12, 12) SWBNNT, (f) top view of MoS_2-doped (10, 10) SWBNNT, and (g) side view of MoS_2-doped (10, 10) SWBNNT. The green balls represent N atoms, the red balls represent B atoms, and the yellow balls represent Mo atoms, while the black balls represent S atoms.

WS_2-doped BNNT systems were missing and therefore need to be investigated. To fill this gap, this research study investigated the photocatalytic properties of the MoS_2-doped system with the SWBNNT structure for water-splitting applications. However, untreated BNNTs cannot be used directly as photocatalysts due to their large band gaps.[7] The reported band gaps of the pristine BNNTs were in the range of 5−6.4 eV,[8] so these values must be narrowed to the range of 1.2−2.8 eV, which is the range of band gaps of semiconductors classified as catalysts that can be used for hydrogen production by photochemical water splitting.[9] It was found that BNNTs with a small excess of boron or carbon substitution can be used as candidates for the preparation of photocatalysts because their optical absorptions are within the spectral range. Nevertheless, the photocatalytic efficiency of the C- or B-substituted BNNT for the evolution of H_2 under visible light was not satisfactory. When the photocatalytic potential of nitrogen-doped BNNT was investigated in air and water media, it was found that the photocatalytic activity of the doped system for H_2 and O_2 evolution showed no significant change after 20 days. Therefore, it is an interesting challenge to improve the photocatalytic activity of BNNTs for H_2 production in the research field of related energy sources. To find solutions to the problems already highlighted, it is necessary to narrow the band gap of the BNNT so that it can efficiently serve as a candidate for next-generation photocatalytic water splitting. Therefore, this research study investigated the photocatalytic properties of the SWBNNT doped with MoS_2 for water splitting. MoS_2 was chosen as our model to dope SWBNNT because of its widely reported photostability, high reactivity, strong oxidizing ability, chemical inertness, photothermal properties, and chemical stability.[10]

2. RESEARCH METHODS

Density functional theory (DFT) calculations were performed using the Perdew−Burke−Ernzerhof (PBE) parametrized exchange−correlation functional by using quantum ESPRESSO (QE) simulation codes.[11] QE is a code operated under the GNU General Public License for materials modeling and electronic structure calculation based on the pseudopotential DFT plane wave approach. QE can perform different tasks, which include ground-state calculation, structural optimization, transition states and minimum energy paths, density-functional perturbation theory response properties, such as phonon frequencies, electron−phonon interactions, and Electron Paramagnetic Resonance (EPR) and Nuclear Magnetic Resonance (NMR) chemical shifts, ab initio molecular dynamics: Car−Parrinello and Born−Oppenheimer MD, spectroscopic properties, quantum import, and generation of pseudo potentials. To ensure accurate results, the quasi-particle energy correction was performed via the G_0W_0 approximation implemented in the Yambo code by using the many-body perturbation theory (MBPT). We used the MBPT to link N atom and N and N ± 1-particle systems using the central time-ordered Green function,[12] given by

$$G(r't', r't') \quad (1)$$

In order to eliminate the underestimation of the band gap by the generalized gradient approximation (GGA) functional, the PBE functional was corrected using the popular GW approximations implemented in Yambo.[13] The 1 × 1 × 30 *k*-point sample was used to describe the Brillouin zone (BZ) for the doped SWBNNT structure. The kinetic energy limit of 40 Ry was used, and the energy convergence criterion of 10−3 Ry was used to reduce computational costs. The electronic band structures of the bare SWBNNT and MoS_2-doped SWBNNT systems were calculated by fixing the Fermi level at

https://doi.org/10.1021/acsomega.3c05907
ACS Omega 2023, 8, 38632−38640

the gamma point of the Brillouin zone. VBM, CBM, and the Fermi level were calculated from the relationship[14]

$$\mathrm{VBM} = \mathrm{VBM}_{\mathrm{cal}} - V_{\mathrm{vac,ns}} \tag{2}$$

$$\mathrm{CBM} = \mathrm{CBM}_{\mathrm{cal}} - V_{\mathrm{vac,ns}} \tag{3}$$

$$E_{\mathrm{f}} = E_{\mathrm{f\,cal}} - V_{\mathrm{vac,ns}} \tag{4}$$

where X_{cal} (X = VBM, CBM, and E_{f}) and V_{vac} are the calculated values of parameters obtained via PBE and the vacuum level potentials of the nanotubes, respectively. The determination of the photocatalytic properties of the investigated systems was carried out by taking into account the optical response of the nanotubes to the incident electromagnetic photon. The complex dielectric function $\varepsilon(\omega)$ was used to determine the optical response of the hybrid SWBNNT via the Bethe-Salpeter Equation (BSE) approach. The value of $\varepsilon(\omega)$ is calculated using the equation[15]

$$\varepsilon(\omega) = \varepsilon_1(\omega) + \varepsilon_2(\omega) \tag{5}$$

where $\varepsilon_1(\omega)$ is the real part and $\varepsilon_2(\omega)$ is the imaginary part of the optical dielectric constant obtained by the Kramers–Kronig relations

$$\varepsilon_2(\omega) = 1 + \frac{2}{\pi} P \int_{\infty}^{0} \frac{\omega' \epsilon_2(\omega)}{(\omega'^2 - \omega^2)} \mathrm{d}\omega' \tag{6}$$

We used the imaginary part of the dielectric function result of the summation of the valence to conduction band transitions under a specified k-point of the corresponding BZ to find the magnitude of the energy absorbed within the visible spectrum.

3. RESULTS AND DISCUSSION

3.1. Structural Optimizations and Elastic Properties.

The pristine unit cell of the armchair single-walled boron nitride nanotubes (SWBNNTs) was optimized from the generated carbon nanotube structure via the Tubegen database.[16] To ensure good stability of the optimized nanotubes, (8, 8), (9, 9), (10, 10), (11, 11), and (12, 12) armchair configurations were studied, and the bond lengths were adjusted to the experimental value of 1.71 Å.[17] It was found that only (10, 10) and (12, 12) SWBNNTs were stable toward MoS_2 doping. The SWBNNTs were doped by exchanging B and N atoms at appropriate positions. The optimized structure is such that one N atom has been replaced by one Mo atom at position 11.14 Å, while two adjacent B atoms have been replaced by two S atoms at positions 12.51 and 10.43 Å, respectively, which brought the concentration of the MoS_2 dopant to 5.7%. The optimized structures of the pristine SWBNNT and MoS_2-doped SWBNNT are presented in Figure 1, while Table 1 presents the sampled k-points relative to the structural optimization of the studied systems.

As can be seen in Table 1, doping the pristine SWBNNT with MoS_2 does not significantly change the stability of the system. However, a small change in diameter was observed because the size of the dopants and the Mo–S bond length are slightly larger compared to the size of both the B and N atoms. In addition, doping of the study material has a significant impact on its volume. Due to this stability,[18] we selected this optimized material as a representative case study of our research.

Table 1. Sampled k-Points with Respect to Doped and Undoped SWBNNT Systems

material	diameter (Å)	volume (Å^3)	k-points
pristine SWBNNT (8, 8)	13.91	0.93	1_1_50
pristine SWBNNT (9, 9)	13.95	0.96	1_1_50
pristine SWBNNT (10, 10)	14.05	1.00	1_1_60
pristine SWBNNT (11, 11)	14.26	1.01	1_1_60
pristine SWBNNT (12, 12)	14.29	1.02	1_1_60
MoS_2-doped SWBNNT (10, 10)	14.42	1.03	1_1_60
pristine SWBNNT (12, 12)	15.37	1.05	1_1_80
MoS_2-doped SWBNNT (12, 12)	15.71	1.08	1_1_80

The chirality of the pristine SWBNNT system was calculated from the equation of the chiral vector for nanotubes. Just like carbon nanotubes,[19] the diameters of armchair SWBNNTs can be obtained by

$$d = \frac{\mathrm{a}}{\pi}\sqrt{n^2 + nm + m^2} \tag{7}$$

where a is the lattice constant in armchair SWBNNT. Different chiralities of armchair SWBNNT were tested before choosing the representative (12, 12) SWBNNT material. Table 2 presents the results obtained for (8, 8), (9, 9), (10, 10), (11, 11), and (12, 12) armchair SWBNNTs.

Table 2. Optimized Chiral Geometry of Armchair SWBNNT

chirality (n, m)	diameter of B (Å)	diameter of N (Å)	B–N bond length (Å)	strain energy (eV/atom)	band gap (eV)
(8, 8)	9.80	9.21	1.70	0.238	4.71
(9, 9)	9.81	9.22	1.71	0.393	4.10
(10, 10)	9.81	9.31	1.73	0.051	5.20
(11, 11)	9.83	9.33	1.73	0.028	5.50
(12, 12)	9.85	9.35	1.75	0.14	5.61

It is evident from Table 2 that the obtained band gaps for (8, 8) and (9, 9) SWBNNT were below the experimental values reported for SWBNNT structures (5 6.3 eV).[20] Although these nanotubes were also found to be stable, their interactions with the MoS_2 dopant did not result in a well-converged value of the total energy. In the case of (10, 10), (11, 11), and (12, 12), well-converged results were obtained for both the band gap values and the lattice parameters. Interactions of these nanotubes led to well-converged total energy values. Therefore, it is necessary to perform our calculations on these nanotube configurations.

The elastic properties of the considered nanotubes were calculated considering the total energy calculations for the (12, 12) SWBNNT and the MoS_2-doped SWBNNT, respectively. We obtained the results of the total energy as a function of volume and different bond lengths and then calculated Young's moduli of the two nanotubes. Figure 2 shows the calculated variations in total energy with volume for the two systems studied. For pure SWBNNT, the total energy decreased with volume from −268.05 to −268.35 eV and then varied directly with volume from 1400 a.u^3, which is in accordance with the obtained experimental and theoretical data.[21] A similar case was observed for the MoS_2-doped SWBNNT, except that in this case, the volume is larger than the volume of pristine SWBNNT because the diameter increases as a result of MoS_2

https://doi.org/10.1021/acsomega.3c05907
ACS Omega 2023, 8, 38632−38640

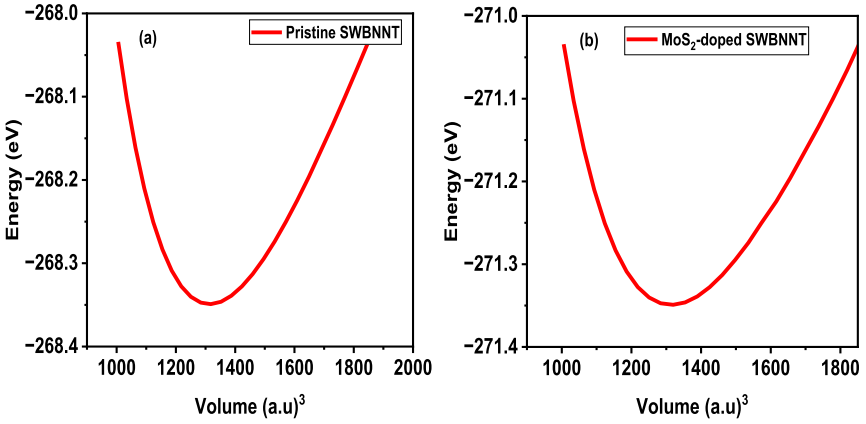

Figure 2. Variation of total energy with volume for (a) pristine SWBNNT and (b) MoS_2-doped SWBNNT.

doping. It was also found that MoS_2 impurity doping does not affect the mechanical stability of the optimized SWBNNT.

Figure 3a,b shows the results of total energy variations with bond lengths for pristine SWBNNT and MoS_2-doped

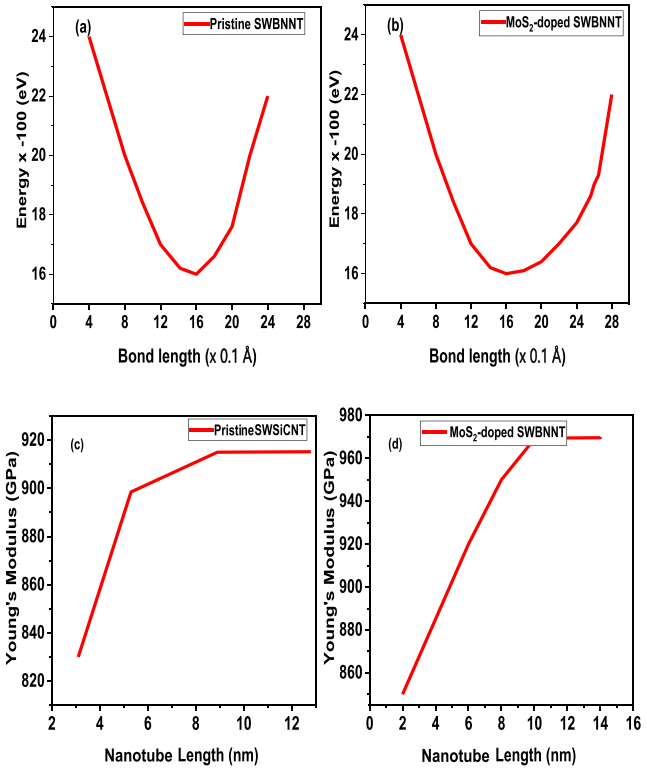

Figure 3. Variations of potential energy with a bond length of (a) pristine SWBNNT and (b) MoS_2-doped SWBNNT. Variations of Young's moduli with nanotubes' length of (c) pristine SWBNNT and (d) MoS_2-doped SWBNNT.

SWBNNT. As can be seen in Figure 3a, the closest distance between adjacent N−B atoms (N−B bond length) is 1.65 nm, which agrees with the obtained experimental value of 1.653 nm.[22] In the case of the MoS_2-doped system shown in Figure 3b, a slight difference of 1.66 nm was obtained due to the doping because of the longer Mo−S bond length than B−N.

To investigate Young's moduli of the systems under study, we use the conventional definition of Young's modulus as

$$Y = \frac{1}{V_0}\frac{\partial^2 E}{\partial^2 \varepsilon} \tag{8}$$

where V_0 is the volume of the given nanotube cylinder defined by[23]

$$V_0 = 2\pi L_0 R \delta R \tag{9}$$

where L_0, R, and δR are the lengths of the nanotube corresponding to its equilibrium volume and ε is the axial strain of the nanotube. The results of the calculated Young's moduli for the pristine and doped systems of SWBNNT structures are shown in Figure 3c,d. It can be seen that Young's moduli are related to the length of the nanotubes. In the case of the pristine (12, 12) SWBNNT, it can be seen that there is a direct variation of Young's modulus with the length of the nanotubes from 825.2 to 899.6 GPa with the lengths from 3.1 to 4.9 nm. Claims for this are attributed to the effects of the cohesive energy of the nanotube being greater than its length. The behavior observed in this case is similar to the observed behavior found for (n, 0) carbon nanotubes.[24] Concerning the doped SWBNNT, there was more energy variation with the length of the nanotubes, which can be seen starting at 850 GPa and extending up to 953 GPa, which is much larger than the range obtained for the original SWBNNT. Based on this, the MoS_2-doped SWBNNT can be considered stiffer than the pristine SWBNNT.

3.2. Effects of MoS_2 Doping on the Electronic (Photocatalytic) Properties of SWBNNT. To better understand the photocatalytic behavior of the doped SWBNNT structure, it is necessary to analyze the electronic behavior of the system under doped and undoped conditions. The electronic properties of the pristine SWBNNT and the MoS_2-doped SWBNNT were studied separately, and the results are shown in Figure 4. Furthermore, all calculations of the electronic transport systems were performed on the (10, 10) and (12, 12) nanotubes. This is intended to ensure that the nanotube, which is suitable as a photocatalyst, has a precise geometry that is as precise as possible. Figure 4a shows the electronic band structure of the pristine SWBNNT. As can be seen, a band gap of 4.9 eV was obtained with the GGA function. However, this does not agree well with the band gap range (5−6.3 eV) obtained for larger SWBNNT, and hence, the GGA results are inconsistent.[25] To correct this inconsistency, we further performed the calculation with the hybrid G_0W_0 approximation to perform a quasi-particle correction via the many-body perturbation theory approach.

https://doi.org/10.1021/acsomega.3c05907
ACS Omega 2023, 8, 38632−38640

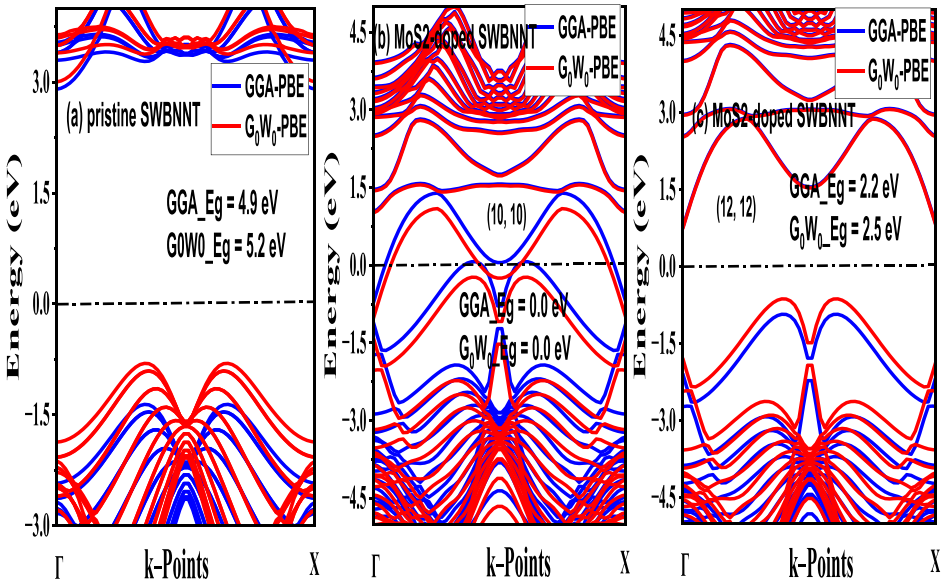

Figure 4. Electronic band structures of (a) pristine SWBNNT, (b) (10, 10) MoS_2-doped SWBNNT, and (c) (12, 12) MoS_2-doped SWBNNT.

A band gap of 5.2 eV was achieved with this method, which is in good agreement with the literature results obtained.[26] Furthermore, the (10, 10) SWBNNT was first doped with MoS_2, and the resulting electronic properties were determined. There were three atoms, one from Mo and two from S elements, that were used to build the doped system, which brought the concentration of the MoS_2 dopant to 6%. The Mo atom was used to replace a B atom, while the two S atoms replaced N atoms. Figure 4b shows the results of the calculated electronic structure of the (10, 10)-MoS_2-doped SWBNNT structure. In terms of its photocatalytic potential, this system can be considered unsuitable for hydrogen photocatalysts since the band gap has been completely closed due to doping, as shown by both GGA and G_0W_0 approximations. To investigate this further, we performed the same investigations of the MoS_2-doped SWBNNT system of the (12, 12) armchair configurations and obtained favorable results.

The doping of MoS_2 in the (12, 12) SWBNNT generated molecular interactions in the doped system that are related to the behavior of the B and N atoms under the quantum mechanical effects of the nanotube diameter. This leads to partial occupation of the VBM by many electrons from the MoS_2 atoms. As a result of this, the band gap of the pure SWBNNT has been narrowed to 2.2 and 2.5 eV by GGA and G_0W_0, respectively. Although both results fall within the band gap range of the photocatalyst, the GGA value was an underestimate, while the G_0W_0 value gives the exact band gap obtained. Furthermore, the band gap obtained is direct since VBM and CBM all have the same momentum.[27] As can be seen, the CBMs of the MoS_2-doped SWBNNT are larger than the H^+/H_2 potential (−4.40 eV), so they are suitable photocatalysts for the half-reaction of hydrogen reduction.[28] Based on the obtained results, it can be shown that the (12, 12) MoS_2-doped SWBNNT semiconductor can be an excellent candidate for enhanced photocatalytic water splitting.

Table 3 presents the optimized lattice parameters, the formation energies, and the band gaps of the (10, 10), (12, 12) and the MoS_2-doped (10, 10), (12, 12) SWBNNT nanostructures. As shown in Table 3, swapping B and N atoms does not significantly affect the stability of the

Table 3. Calculated Band Gap Energies, Lattice Parameters, and Formation Energies of Pristine and Doped Systems under Studies

parameters	pristine (10, 10) SWBNNT	MoS_2-doped (10, 10) SWBNNT	pristine (12, 12) SWBNNT	MoS_2-doped (12, 12) SWBNNT
band gap (eV)	5.20	0.00	5.40	2.50
a (Å)	38.00	39.00	39.31	39.50
b (Å)	38.00	39.00	39.31	39.50
c (Å)	0.12	0.13	0.14	0.14
A	90.00	90.00	90.00	90.00
B	90.00	90.00	90.00	90.00
Γ	120	120	120	120
formation energy (eV/unit)	−8.37	−8.71	−8.42	−8.71

SWBNNT. However, the band gap value decreased to zero for (10, 10) MoS_2-doped SWBNNT, whereas the band gap value decreased to 2.5 eV after doping (12, 12) SWBNNT with MoS_2, which is in good agreement with the experimental values of the band gaps for other photocatalysts.[29] The band gap of the MoS_2-doped (12, 12) SWBNNT was narrowed in the energy range of 0.6−1.8 eV due to the presence of vacant MoS_2 orbitals. In addition, the CBMs of the doped system consist of the combination of the vacant orbitals of the Mo and S atoms, respectively.

To understand the electronic occupations and orbital contributions of atoms in the doped systems of the (10, 10) and (12, 12) SWBNNT systems, we calculated both the total density of states (TDOS) and the partial density of states (PDOS) of the interacting systems. Figure 5 shows the results in detail. In the case of the pure SWBNNT shown in Figure 5a, TDOS is divided into three regions. The first two ranges in the −10 to −8 and −1.6 to 6 eV range fall in the valence band, while the third range in the 2.8−5 eV range is in the conduction band. The Fermi level showed the existence of empty states, and this justified the system as a semiconductor. Therefore, the behavior of this nanotube is determined by these three domains. The TDOS in Figure 5b shows occupied

https://doi.org/10.1021/acsomega.3c05907
ACS Omega 2023, 8, 38632−38640

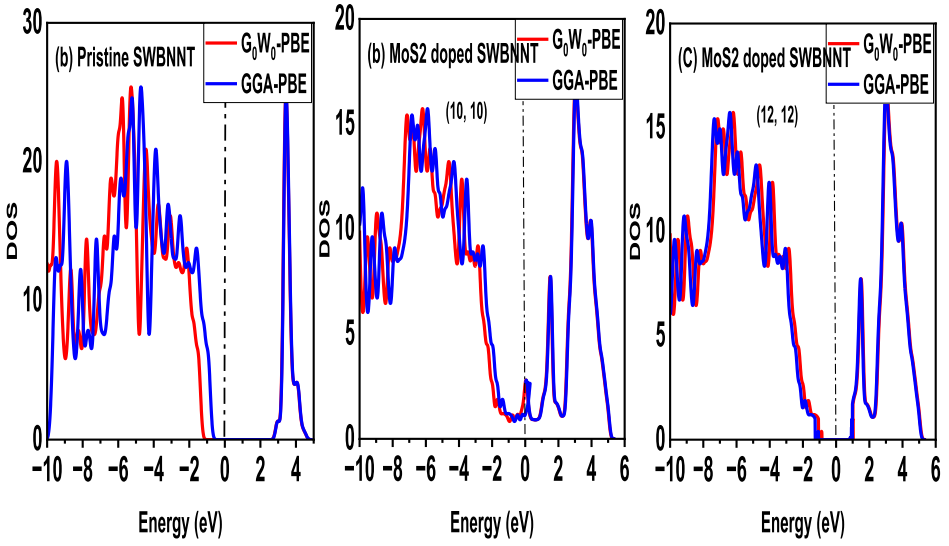

Figure 5. TDOS diagrams of (a) pristine (10, 10) SWBNNT, (b) MoS_2-doped (10, 10) SWBNNT, and (c) MoS_2-doped (12, 12) SWBNNT.

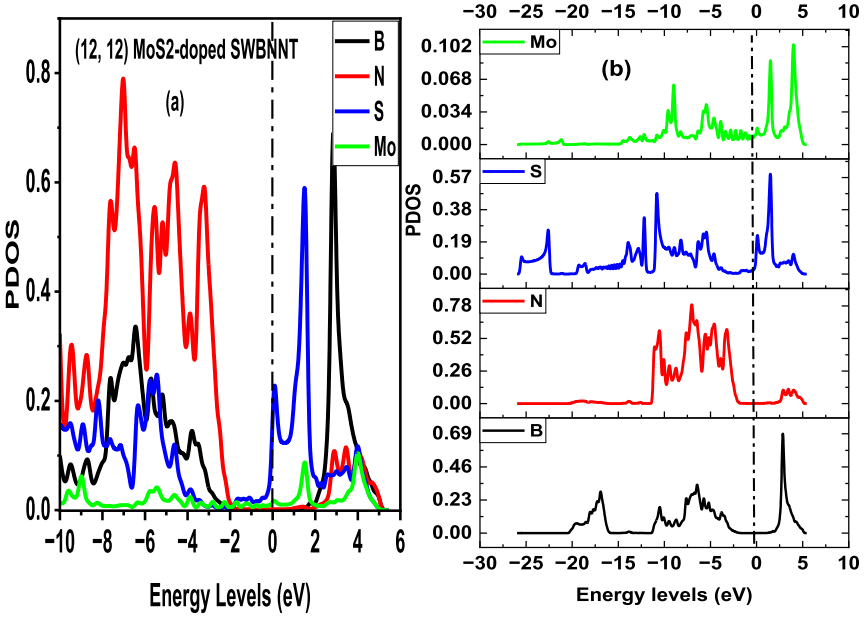

Figure 6. PDOS diagrams for (a) the (12, 12) MoS_2-doped SWBNNT and (b) separate orbital contributions on the (12, 12) MoS_2-doped SWBNNT.

states at the Fermi level as a result of MoS_2 doping. In the case of (12, 12) MoS_2-doped SWBNNT, Figure 5c shows that the VBM is −10.2 eV, which is close to the value of an ideal water-splitting photocatalyst. Therefore, the (12, 12) MoS_2-doped SWBNNT is a suitable photocatalyst for the entire water-splitting process under sunlight irradiation. Moreover, due to the nature of its VBM, this material can also be used as an ideal n-type photocatalyst in a heterojunction water splitting.[30] Different orbital contributions from each interacting atom are shown in Figure 6a,b. In addition, the orbital combinations of the VBM and CBM of this nanotube are given in Table 3. The VBM is mainly dominated by the 2p orbitals of S and the 4f orbitals of Mo atoms, respectively. Furthermore, the effects of the vacant 2p orbitals of B and N atoms in the doped SWBNNT increased with increasing energy levels. In general, the photocatalytic behavior of the MoS_2-doped SWBNNT semiconductor is governed by the quantum mechanical effects of the 2p and 4f orbitals of S and Mo atoms, respectively, and this can be explained by the occupation of the Fermi level by S and Mo orbitals as shown in Figure 6b.

3.3. Effects of Photoabsorption of the MoS_2-Doped SWBNNT (Photocatalysts). Photocatalysts absorb electromagnetic energy (solar radiation) in the visible range. Their photocatalytic nature depends on light absorption and charge transport. The number of active sites related to the size of the band gap also plays a key role in the behavior of the photocatalyst. The imaginary dielectric constant was considered to explain the light energy absorbed by the MoS_2-doped SWBNNT. Figure 7 shows the calculated real and imaginary dielectric values related to the energy scattered and absorbed by the pristine and doped systems of (12, 12) SWBNNTs. Calculations were performed using the G_0W_0-BSE approximation, which takes into account both electron−electron and electron−hole interactions.[31] The real dielectric functions

https://doi.org/10.1021/acsomega.3c05907
ACS Omega 2023, 8, 38632−38640

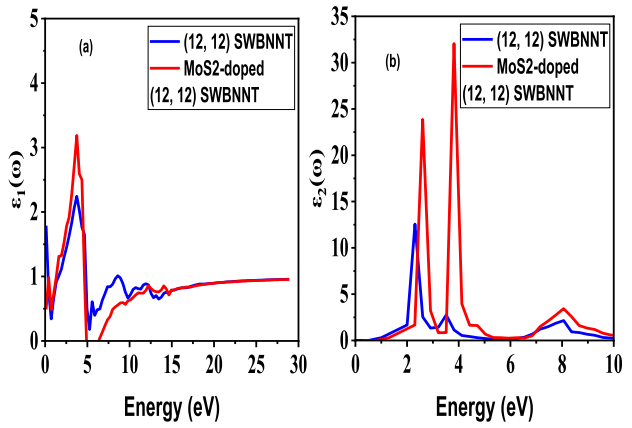

Figure 7. (a) Real dielectric spectra of the pristine and MoS_2-doped SWBNNT structures and (b) imaginary dielectric spectra of the pristine and MoS_2-doped SWBNNT structures.

determine the amount of light energy that is scattered or reflected by the photoabsorbing material. For the MoS_2-doped SWBNNT system, Figure 7a shows the real dielectric spectrum that accounts for the energy reflected in the system. As can be seen, there is generally less reflection in the visible region, corresponding to the rise and fall of the lower peaks between 0 and 2.4 eV. Therefore, the system absorbs more energy than it reflects. Figure 7b shows the amount of energy absorbed by the pristine and doped systems. In both systems, the optical absorption edge starts at 2.6 eV, which is within the visible range of absorbed electromagnetic energy and is comparable to the available literature values, as shown in Table 4. However,

Table 4. Photocatalytic Band Gap and Optical Absorption Edge of the System under Study and the Obtained Literature

material	band gap (eV)	absorption edge (eV)	binding energy (eV)	references
MoS_2-doped SWBNNT	2.50	2.60	−8.71	current work
N-doped TiO_2	2.91	2.61	−7.21	32
nanotube/TiO_2−ZnO composites	2.31	2.59	−7.43	33
2D MoS_2	1.30	1.45	−6.61	34
MoS_2/Ni_3S_2	1.48	1.51	−7.33	35

the amount of energy absorbed by the pristine SWBNNT system is much less than that of the energy absorbed by the MoS_2-doped SWBNNT. In addition, the presence of two higher peaks falls to 2.3 and 3.1 eV, respectively, by the MoS_2-doped system. This showed that the MoS_2-doped SWBNNT absorbs the highest amount of visible solar radiation, revealing a greater degradation of chemicals or pollutants. Furthermore, the higher absorption by MoS_2-doped SWBNNT was due to the quantum effects and band transitions through the orbitals of Mo and S atoms. Therefore, MoS_2-doped SWBNNT may be a better candidate for next-generation photocatalysts for overall water splitting.

4. CONCLUSIONS

In this work, the photocatalytic properties of the SWBNNT's MoS_2-doped system were investigated using the popular DFT as implemented in QE and Yambo simulation codes. The material stabilities were checked for different chiralities of the pristine armchair SWBNNT before doping, and it was found that only (12, 12) SWBNNT was suitable for MoS_2 doping for photocatalysis. The doping of MoS_2 in the (12, 12) SWBNNT system generated molecular interactions in the doped system, and they are related to the behavior of the B and N atoms under the quantum mechanical effects of the nanotube diameter. This leads to the partial occupation of the VBM by many electrons from the MoS_2 atoms. This narrowed the band gap of the pure SWBNNT to 2.2 and 2.5 eV by GGA and G_0W_0, respectively. The system absorbs more energy than it reflects. In both the pure and doped systems, the optical absorption edge starts at 2.6 eV, which is within the electromagnetic energy absorbed in the visible range and this also falls within the energy absorption range of other photocatalysts. These properties and other novel features observed in MoS_2-doped SWBNNT made it a better candidate for next-generation photocatalysts for overall water splitting.

■ ASSOCIATED CONTENT

Data Availability Statement

All data are available in the manuscript.

■ AUTHOR INFORMATION

Corresponding Author

Mayeen Uddin Khandaker − *Centre for Applied Physics and Radiation Technologies, School of Engineering and Technology, Sunway University, 47500 Bandar Sunway, Selangor, Malaysia; Faculty of Graduate Studies, Daffodil International University, 1216 Dhaka, Bangladesh;* orcid.org/0000-0003-3772-294X; Email: mayeenk@diu.edu.bd, mu_khandaker@yahoo.com

Authors

Yahaya Saadu Itas − *Department of Physics, Bauchi State University Gadau, 751105 Gadau, Bauchi, Nigeria*

Abdussalam Balarabe Suleiman − *Department of Physics, Federal University, 720223 Dutse, Nigeria*

Chifu E. Ndikilar − *Department of Physics, Federal University, 720223 Dutse, Nigeria*

Abdullahi Lawal − *Department of Physics, Federal College of Education Zaria, 810282 Kaduna, Nigeria*

Razif Razali − *Department of Physics, Faculty of Science, Universiti Teknologi Malaysia, 81310 Johor Bahru, Johor, Malaysia*

Md Habib Ullah − *Department of Physics, American International University-Bangladesh (AIUB), 1229 Dhaka, Bangladesh*

Hamid Osman − *Department of Radiological Sciences, College of Applied Medical Sciences, Taif University, 21944 Taif, Saudi Arabia*

Complete contact information is available at: https://pubs.acs.org/10.1021/acsomega.3c05907

Author Contributions

Y.S.I. developed the concept and wrote the main manuscript, A.B.S., A.L., R.R., M.U.K., M.H.U., and H.O. reviewed the manuscript, C.E.N. supported the theoretical methodology, R.R. provided the materials and computational packages, A.L. and M.U.K. provided technical, theoretical, and conceptual reviews.

Notes

The authors declare no competing financial interest.

https://doi.org/10.1021/acsomega.3c05907
ACS Omega 2023, 8, 38632−38640

■ ACKNOWLEDGMENTS

The authors of this work acknowledge Bauchi State University, Gadau, Nigeria, for providing the resource persons and funds for the successful takeoff of this research study. Federal University Dutse-Nigeria and Universiti Teknologi Malaysia provided the computational condensed matter training to the lead researcher.

■ REFERENCES

(1) Zhang, Z.-Y.; Tian, H.; Bian, L.; Liu, S.-Z.; Liu, Y.; Wang, Z.-L. Cu-Zn-based alloy/oxide interfaces for enhanced electroreduction of CO2 to C^{2+} products. *J. Energy Chem.* **2023**, *83*, 90−97.

(2) Luo, M.; Yang, J.; Li, X.; Eguchi, M.; Yamauchi, Y.; Wang, Z.-L. Insights into alloy/oxide or hydroxide interfaces in Ni-Mo-based electrocatalysts for hydrogen evolution under alkaline conditions. *Chem. Sci.* **2023**, *14*, 3400−3414.

(3) Bhattacharjee, S.; Bera, S.; Das, R.; Chakraborty, D.; Basu, A.; Banerjee, P.; Ghosh, S.; Bhaumik, A. A Ni(II) Metal-Organic Framework with Mixed Carboxylate and Bipyridine Ligands for Ultrafast and Selective Sensing of Explosives and Photoelectrochemical Hydrogen Evolution. *ACS Appl. Mater. Interfaces* **2022**, *14*, 20907−20918.

(4) Bera, S.; Kumari, A.; Ghosh, S.; Basu, R. N. Assemble of Bi-doped TiO_2 onto 2D MoS_2: an efficient p-n heterojunction for photocatalytic H2 generation under visible light. *Nanotechnology* **2021**, *32*, 195402.

(5) Bera, S.; Samajdar, S.; Pal, S.; Das, P. S.; Jones, L. A.; Finch, H.; Dhanak, V. R.; Ghosh, S. Effect of metal doping in Bi_2WO_6 microflowers for enhanced photoelectrochemical water splitting. *Ceram. Int.* **2022**, *48*, 35814−35824.

(6) Itas, Y. S.; Suleiman, A. B.; Ndikilar, C. E.; Lawal, A.; Razali, R.; Khandaker, M. U.; Ahmad, P.; Tamam, N.; Sulieman, A. The exchange-correlation effects on the electronic bands of hybrid armchair single-walled carbon boron nitride nanostructure. *Crystals* **2022**, *12* (3), 394.

(7) Itas, Y. S.; Suleiman, A. B.; Ndikilar, C. E.; Lawal, A.; Razali, R.; Idowu, I. I.; Khandaker, M. U.; Ahmad, P.; Tamam, N.; Sulieman, A.; et al. Computational Studies of the Excitonic and Optical Properties of Armchair SWCNT and SWBNNT for Optoelectronics Applications. *Crystals* **2022**, *12* (6), 870.

(8) Soares, G. P.; Guerini, S. Structural and Electronic Properties of Impurities on Boron Nitride Nanotube. *J. Mod. Phys.* **2011**, *2* (8), 6821.

(9) Ansari, S. A.; Cho, M. H. Highly Visible Light Responsive, Narrow Band gap TiO_2 Nanoparticles Modified by Elemental Red Phosphorus for Photocatalysis and Photoelectrochemical Applications. *Sci. Rep.* **2016**, *6*, 25405.

(10) Salimi, M.; Shokrgozar, M. A.; Hamid, D. H.; Vossoughi, M. Photothermal properties of two-dimensional molybdenium disulfide (MoS_2) with nanoflower and nanosheet morphology. *Mater. Res. Bull.* **2022**, *152*, 111837.

(11) Itas, Y. S.; Suleiman, A. B.; Ndikilar, C. E.; Lawal, A.; Razali, R.; Idowu, I. I.; Khandaker, M. U. DFT studies of structural, electronic and optical properties of (5, 5) armchair magnesium oxide nanotubes (MgONTs). *Phys. E* **2023**, *149*, 115657.

(12) Rocca, D.; Gebauer, R.; Saad, Y.; Baroni, S. Turbo charging time-dependent density-functional theory with Lanczos chains. *J. Chem. Phys.* **2008**, *128*, 154105.

(13) Kim, S.; Lebègue, S.; Ringe, S.; Kim, H. GW Quasiparticle Energies and Bandgaps of Two-Dimensional Materials Immersed in Water. *J. Phys. Chem. Lett.* **2022**, *13* (32), 7574−7582.

(14) Jouypazadeh, H.; Farrokhpour, H.; Momeni, M. M. A DFT study of the water-splitting photocatalytic properties of pristine, Nb-doped, and V-doped Ta3N5 monolayer nanosheets. *Surface. Interfac.* **2021**, *26*, 101379.

(15) Aminu Yamusa, S.; Shaari, A.; Isah, I.; Bello Ibrahim, U.; Kunya, S.; Abdulkarim, S.; Itas, Y. S.; Alsalamh, M. Effects of Exchange Correlation Functional (Vwdf3) on the Structural, Elastic, and Electronic Properties of Transition Metal Dichalogenides. *J. Niger. Soc. Phys. Sci.* **2023**, *5* (1), 1094.

(16) Lee, S. U.; Mohammad, K.; Fabio, P. Electron transport through carbon nanotube intramolecular heterojunctions with peptide linkages. *Phys. Chem. Chem. Phys.* **2008**, *10* (34), 5225−5231.

(17) Itas, Y. S.; Ndikilar, C. E.; Zangina, T.; Hafeez, H. Y.; Safana, A. A.; Khandaker, M. U.; Ahmad, P.; Abdullahi, I.; Olawumi, B. K.; Babaji, M. A.; et al. Synthesis of Thermally Stable h-BN-CNT Hetero-Structures via Microwave Heating of Ethylene under Nickel, Iron, and Silver Catalysts. *Crystal* **2021**, *11* (9), 1097.

(18) Itas, Y. S.; Baballe, A.; Danmadami, A. M.; Yahaya, S. A. Analysis of different welding speeds and the micro structure on the welded joints of silicon steel pipe. *IOP Conf. Ser.: Mater. Sci. Eng.* **2020**, *932* (1), 012123.

(19) Itas, Y. S.; Tasiu, Z.; Ndikilar, C. E. Carbon Nanotubes: A Review of Synthesis and Characterization Methods/Techniques. *Int. J. Sci. Technol.* **2020**, *8* (2), 44.

(20) Kayang, K. W.; Nyankson, E.; Efavi, J. K.; Abavare, E.; Garu, G.; Onwona-Agyeman, B.; Yaya, A. Single-Walled boron nitride nanotubes interaction with nickel, titanium, palladium, and gold metal atoms- A first-principles study. *Results Mater.* **2019**, *2*, 100029.

(21) Petrushenko, I. K. DFT Study on Structural and Mechanical Properties of Single-walled Carbon and Boron Nitride Nanotubes Functionalized with Carbenes. *J. Nano- Electron. Phys.* **2016**, *8* (3), 03031.

(22) Ansari, R.; Faghihnasiri, M.; Malakpour, S.; Sahmani, S. A DFT study of elastic and structural properties of (3,3) boron nitride nanotube under external electric field. *Superlattice. Microst.* **2015**, *82*, 90−102.

(23) Fereidoon, A.; Ghorbanzadeh Ahangari, M.; Ganji, M. D.; Jahanshahi, M. Density functional theory investigation of the mechanical properties of single-walled carbon nanotubes. *Comput. Mater. Sci.* **2012**, *53* (1), 377−381.

(24) Liang, Y.; Han, Q.; Xin, H. Elastic Properties of Carbon Nanotubes. *J. Comput. Theor. Nanosci.* **2013**, *10*, 1061−1071.

(25) Saadu Itas, Y.; Suleiman, A. B.; Ndikilar, C. E.; Lawal, A.; Razali, R.; Idowu, I. I.; Khandaker, M. U. Effects of oxygen absorption on the electronic and optical properties of armchair and zigzag Silicon Carbide Nanotubes (SiCNTs). *Phys. Scr.* **2022**, *98* (1), 015824.

(26) Gomes, F.; Dmitriev, V.; Nascimento, C. Analysis of electronic structure of boron nitride nanotubes with different positions of intrinsic impurities. *J. Microwaves, Optoelectron. Electromagn. Appl.* **2014**, *13* (2), 214−222.

(27) Itas, Y. S.; Suleiman, A. B.; Yamusa, A. S.; Razali, R.; Danmadami, A. M. Ab'initio studies of the structural and electronic properties for single-walled armchair MgONT, SiCNTs and ZnONTs for next generations' optoelectronics. *Gadau Journal of Pure and Allied Sciences* **2022**, *1* (2), 160−165.

(28) Guo, S.; Li, X.; Li, J.; Wei, B. Boosting photocatalytic hydrogen production from water by photothermally induced biphase systems. *Nat. Commun.* **2021**, *12*, 1343.

(29) Nair, R. V.; Gummaluri, V. S.; Matham, M. V.; Vijayan, C. A review on optical bandgap engineering in TiO2 nanostructures via doping and intrinsic vacancy modulation towards visible light applications. *J. Phys. D: Appl. Phys.* **2022**, *55* (31), 313003.

(30) Kianipour, S.; Razavi, F. S.; Hajizadeh-Oghaz, M.; Abdulsahib, W. K.; Mahdi, M. A.; Jasim, L. S.; Salavati-Niasari, M. The synthesis of the P/N-type $NdCoO_3$/g-C_3N_4 nano-heterojunction as a high-performance photocatalyst for the enhanced photocatalytic degradation of pollutants under visible-light irradiation. *Arab. J. Chem.* **2022**, *15* (6), 103840.

(31) Shishkin, M.; Kresse, G. Self-consistent GW calculations for semiconductors and insulators. *Phys. Rev. B: Condens. Matter Mater. Phys.* **2007**, *75*, 235102.

(32) Zhang, Y.; Xu, X. Machine Learning Band Gaps of Doped-TiO_2 Photocatalysts from Structural and Morphological Parameters. *ACS Omega* **2020**, *5* (25), 15344−15352.

(33) Bakos, L. P.; Justh, N.; Moura da Silva Bezerra da Costa, U. C.; László, K.; Lábár, J. L.; Igricz, T.; Varga-Josepovits, K.; Pasierb, P.;

https://doi.org/10.1021/acsomega.3c05907
ACS Omega 2023, 8, 38632−38640

Färm, E.; Ritala, M.; et al. Photocatalytic and Gas Sensitive Multiwalled Carbon Nanotube/TiO_2-ZnO and ZnO-TiO_2 Composites Prepared by Atomic Layer Deposition. *Nanomaterials* **2020**, *10* (2), 252.

(34) Thomas, N.; Mathew, S.; Nair, K. M.; O'Dowd, K.; Forouzandeh, P.; Goswami, A.; McGranaghan, G.; Pillai, S. 2D MoS_2: structure, mechanisms, and photocatalytic applications. *Mater. Today Sustain.* **2021**, *13*, 100073.

(35) Jin, D.; Qiao, F.; Liu, W.; Liu, Y.; Xie, Y.; Li, H. One-step fabrication of MoS_2/Ni_3S_2 with P-doping for efficient water splitting. *CrystEngComm* **2022**, *24*, 4057−4062.

https://doi.org/10.1021/acsomega.3c05907
ACS Omega 2023, 8, 38632−38640